

Catalytic activity of Cu and Co supported on ceria-yttria-zirconia oxides for the diesel soot combustion reaction in the presence of NOx.

María Pilar Yeste^{a,*}, Miguel Ángel Cauqui^a, Javier Giménez-Mañogil^b, Juan Carlos Martínez-Munuera^b, Miguel Ángel Muñoz^a, Avelina García-García^b

^a Grupo de Química de Sólidos y Catálisis/Dpto. de Ciencia de los Materiales e Ingeniería Metalúrgica y Química Inorgánica e Instituto Universitario de Investigación en Microscopía Electrónica y Materiales./Universidad de Cádiz, Puerto Real, España

^b Grupo de Materiales Carbonosos y Medio Ambiente/Dpto. de Química Inorgánica e Instituto Universitario de Materiales./Universidad de Alicante, Sant Vicent del Raspeig, Alicante, España

**Corresponding author, e-mail: pili.yeste@uca.es*

Abstract

In this work, copper and cobalt oxides supported on a ceria-yttria-stabilized zirconia (Ce-YSZ) have been studied as alternative to noble metals for the soot removal in diesel engines. The Ce-YSZ support was activated in order to obtain a catalyst with a high redox performance. The resulting catalysts were characterized by N₂ physisorption, ICP, XRD, TPR-H₂, TPR-CO, HAADF-STEM and XEDS. Additionally, their catalytic performance was evaluated in the NO oxidation to NO₂ and in the combustion of soot in presence/absence of NO_x. The Co/Ce-YSZ catalyst shows a maximum NO₂ production activity higher than 70%, very close to that obtained with a commercial Pt catalyst used as a reference, and largely better than that of Cu/Ce-YSZ. A similar trend is observed in the combustion of soot in the presence of NO_x, thus indicating the prevalence of the NO₂-assisted mechanism for the oxidation of soot when NO₂ is present. Results obtained with unsupported Co₃O₄ and CuO oxides suggest that Co-containing catalyst is not only a better NO₂ generator but also exhibits a more efficient utilization of NO_x. Co₃O₄ entities would act as a *pseudo-platinum phase* allowing fresh supply of NO₂ along the catalytic bed, thus accelerating the soot combustion reaction. However, if NO_x is absent, the order of soot combustion rate matches with the performance in reducibility (“active oxygen” mechanism), the Cu catalyst being the most active in comparison with Co or Pt. Under these conditions, Ce-YSZ supported catalysts benefit from the excellent oxygen-exchange properties of surface Ce-Y-Zr oxide nanostructures.

Keywords: soot combustion; Ce-YSZ support; Cu; Co; NO_x.

1. Introduction

Engine technologies are advancing rapidly in response to the fuel consumption and CO₂ regulations across major markets. A wide range of technology pathways exist, both on the light and heavy-duty side, to meet the upcoming GHG regulations. Government mandates on zero emission vehicles and novel schemes to limit vehicle growth and protection of city centres from pollution are also influencing consumer choices and ultimately OEM (Original Equipment Manufacturers) strategies on improving fleet-wide fuel efficiencies [1].

In heavy-duty applications the range of choices are limited to the ambit of fossil fuel types, with diesel fuel developments still holding an advantage. Therefore, during the past few decades, and probably, in the short term, diesel engines equipped with direct fuel injection will go on as a main power source for passenger cars and other forms of transportations (locomotives, ships and so on...) due to their high durability, improved fuel efficiency, and low cost compared to gasoline engines of similar features [2, 3]. However, PM, as one of the major pollutants can have a strong impact on human respiratory system being carcinogenic in nature [4-7]. Therefore, diesel soot particles need to be eliminated by effective exhaust treatment strategies [8-10]. One of the most effective ones for soot removal in the diesel context is the use of active soot combustion catalysts, which can oxidise soot particles at low ignition temperature (because the exhaust gases from diesel engine are normally in the temperature range of 150°-500°C), and present high thermal stability for further integration in diesel particulate filters (catalysed-DPF) [11,12]. This stimulates the invention of catalytic materials with excellent inherent reactivity. In the effort to design very efficient catalysts, noble metals have been widely investigated as the main components of catalytic systems used for soot oxidation in the presence of NO_x. Despite their great activity, the main drawback in implementing noble metals for this application is the high cost, which limits the economic feasibility and prevents their widespread use in the oxidation of soot [13]. Therefore, to reach the present emission standards of PMs, the search of novel low-cost and highly effective nanostructured catalysts remains a primary challenge [14, 15].

Among various low-cost metal oxides, CeO₂ has been proposed in the catalytic diesel soot

combustion [16-20]. The activity of ceria-based materials depends on their chemical composition, structural features, defects, morphology and particle size generated by doping and non-stoichiometry [21,22]. Among a variety of cerium-containing oxides, pyrochlore-type materials are known as useful and practical materials applied in many fields, and also in catalysis. In the past years, there has been an increasing interest in using pyrochlores as catalysts in several environmental-related processes because of their unique structure with excellent thermal stability and potential catalytic activity in a wide range of temperatures [23]. One alternative to obtain a family of these pyrochlore structures is based on anchoring individual ceria-zirconia nanostructures onto the surface of a carrier material (YSZ). It was recently reported by some of the authors of the present article that these nanostructures present not only an outstanding redox performance as a function of OSC and reducibility [24], but also an impressive stability under high-temperature conditions [25]. The optimum redox properties and catalytic response in oxidation reactions can be further improved with the incorporation of transition metals onto their surfaces.

The aim of this work focuses on the study of these nanostructured ceria-yttria-zirconia materials (CeO₂-YSZ) as supports of copper and cobalt oxides catalysts. These systems have been evaluated in the oxidation of NO to NO₂ and the soot combustion under NO_x/O₂ and O₂. The ability of these catalytic formulations to promote the NO₂-assisted and/or the “active oxygen”-assisted soot combustion is analysed. The catalytic behaviours are compared with those obtained for a Pt/Al₂O₃ commercial catalyst and, finally, the mechanistic implications deduced are presented.

2. Experimental

2.1 Preparation of samples.

A commercial YSZ oxide (Tecnan-Nanommat S.L., 15% molar of Y, $S_{\text{BET}} = 89 \text{ m}^2 \cdot \text{g}^{-1}$) was impregnated with an aqueous solution of Ce(NO₃)₃·6H₂O to obtain the 13% mol CeO₂/YSZ oxide used as support. After impregnation, this oxide was dried overnight at 110°C and further calcined at 500°C for 1 h. The specific surface area of the resulting CeO₂/YSZ oxide was $73 \text{ m}^2 \cdot \text{g}^{-1}$.

This material was activated by using a SRMO-SRSO-SRMO redox-aging cycle already described in previous works [25]. Briefly, it consists on a combination of the following treatments:

- (1) Severe Reduction (SR): heating in H₂(5%)/Ar (60 cm³·min⁻¹) up to 950 °C. After 2 h at this temperature, the gas flow is switched to He (1 h), and finally the sample is cooled down to room temperature.
- (2) Mild Oxidation (MO): heating in O₂ (5%)/He up to 500 °C (1 h), followed by cooling to room temperature.
- (3) Severe Oxidation (SO): heating in O₂ (5%)/He up to 950 °C(1 h), followed by cooling to room temperature.

For all these treatments we used heating rates of 10 °C·min⁻¹ and flow rates of 60 cm³·min⁻¹.

Thus, the activation cycle consisted of 3 consecutive steps: 1° SRMO (SR+MO), 2° SRSO (SR+SO) and 3° SRMO (SR+MO). In order to prevent overheating of the reduced samples, they were always passivated after SR pulsing O₂ (5%)/He at 25 °C. A schematic representation of the complete cycle is included in the Supporting Information (S1).

To illustrate the effect of this activation treatment, Table 1 summarises the Oxygen Storage Capacity (OSC) of the fresh and the activated oxides at 350°C and 500°C. According to these values, the SRMO-SRSO-SRMO treatment significantly improves the OSC in terms of both Ce⁴⁺ reduced to Ce³⁺ and mmol O₂ adsorbed per gram of sample. It should be noted that the percentage of Ce⁴⁺ reduced at low temperature is almost 100% in the cycled sample. This oxide was used as catalytic support and will be hereafter referred as Ce-YSZ.

< near Table 1 >

Cu/Ce-YSZ and Co/Ce-YSZ catalysts were prepared by incipient wetness impregnation of Ce-YSZ, with aqueous solutions of the corresponding nitrates. The Cu and Co molar content was 11%. After

impregnation, the samples were submitted to drying overnight at 110 °C and calcination at 500 °C for 1 h.

2.2 Characterization of the samples.

The chemical composition of the catalysts was determined by using inductively coupled plasma-atomic emission spectrometry (ICP-AES). Textural properties (surface area and porosity) were analysed by N₂ adsorption isotherms at -196 °C, on a Quantachrome Autosorb iQ automatic equipment. Prior to measurements, the samples were degassed at 200 °C for 2 h. The BET method was used to calculate the surface area, and pore volume and width were calculated by the BJH method. Powder X-ray diffraction (XRD) patterns of the catalysts were obtained on a Bruker (D8ADVANCE) diffractometer, with Cu K α radiation (40 kV and 40 mA).

Oxygen storage capacity (OSC) values were estimated from oxygen chemisorption isotherms at 200 °C, in the oxygen partial pressure range 0-300 Torr. The isotherms were recorded on a Micromeritics (ASAP 2020) device. The samples were pre-reduced by heating in 5% H₂/Ar at the selected reduction temperature (350°C or 500°C) for 1 h, then evacuated under vacuum at 500°C (1h) and finally cooled down to 25 °C also under high vacuum, to guarantee the removal of any amount of chemisorbed hydrogen.

H₂-TPR and CO-TPR studies were carried out in an experimental device coupled to a quadrupole mass spectrometer (Pfeiffer, model Thermostar QME-200). The reactive gas compositions were 5% H₂/Ar or 5% CO/He, respectively. Before starting TPR runs, the samples were cleaned under flowing 5% O₂/He at 500 °C for 1h; then, they were cooled down to 150 °C under the same flow and finally to 25 °C in He. Flow rates of 60 cm³·min⁻¹ and heating ramps of 10°C ·min⁻¹ were always used. The results are presented in the form of water (m/z=18) or carbon dioxide (m/z=44) evolution as a function of temperature. Consistency with hydrogen or carbon monoxide consumption profiles was in all cases confirmed.

For the STEM analysis, the samples were dispersed in ethanol and deposited by dripping on carbon-coated TEM grids. HAADF-STEM images were acquired in a FEI Titan3 microscope operated at 300 kV. A semi convergence angle of ~21 mrad was used together with a camera length of 115 mm. Energy Dispersive X-ray Spectroscopy (XEDS) measurements with a resolution at the atomic scale were carried out using the same microscope, which was equipped with a ChemiSTEM system. Analysis was performed using the Bruker ESPRIT software.

2.3 Catalytic Activity measurements.

The catalytic tests were performed at atmospheric pressure in a fixed-bed tubular reactor coupled to specific NDIR-UV gas analysers for NO, NO₂, CO, CO₂ and O₂ determinations (Fisher-Rosemount, models BINOS 100, 1004, 1001).

Catalytic NO oxidation experiments were carried out using 80 mg of catalyst diluted with 320 mg of SiC. For the soot combustion tests, a carbon black from Evonik-Degussa GmbH (Printex-U) was used as model soot. In a typical run, 80 mg of catalyst and 20 mg of soot were mixed with a spatula in the so-called *loose* contact mode. This mixture was further diluted with 300 mg of SiC. In both cases, the reactive gas mixtures contained 0.05% NO_x/5% O₂ (or just 5% O₂ for the case of soot combustion experiments in absence of NO_x) and N₂ as balanced gas. The total flow used was 500 ml·min⁻¹ and the space velocity was 30000 h⁻¹.

3. Results and Discussion

3.1 Characterization of samples

The values of the BET surface area and chemical composition of the samples are gathered in Table 2. The low surface area of these samples is a consequence of the high temperature redox-aging cycles to which they were submitted. Concerning the chemical composition obtained by ICP, both Cu and Co contents are below the nominal values, the difference with respect to these values being slightly higher in the case of Cu. As it can be seen in this table, Cu and Co catalysts show a very similar

surface area, a little bit lower than that obtained for the bare support, probably due to the partial filling of the pores after impregnation.

< near Table 2 >

< near Figure 1 >

Fig. 1 shows the pore size distribution curves of Barrett-Joyner-Halenda (BJH) model for the support and the Cu and Co catalysts. The pore diameters of Cu and Co catalysts mainly distribute within the range 10-30 nm.

Fig. 2 shows the XRD diagrams of the investigated samples. For the Ce-YSZ support, the XRD pattern shows the tetragonal reflections peaks corresponding to the YSZ oxide (JCPDS 30-1468). The absence of peaks corresponding to fluorite CeO₂ suggests that, after the SRMO-SRSO-SRMO activation treatment, the cerium has been incorporated into the YSZ structure, at least at the surface level. This conclusion is supported by the results obtained in a previous study, focused on the investigation of the influence of these singular activation pre-treatments on the structural properties of Ce/YSZ oxides. By using advanced electron microscopy techniques, the formation of surface nanostructures of Ce₂Zr₂O₇ with a pyrochlore-like structure was illustrated [24].

The Cu/Ce-YSZ pattern shows the presence of new diffraction peaks at 35.5° and 38.7° corresponding to the monoclinic structure of CuO (JCPDS 48-1548). In the case of the Co/Ce-YSZ catalyst, reflections at 37° and 65.2° which can be indexed as cubic Co₃O₄ (JCPDS 15-0806) were detected.

< near Figure 2 >

3.2 Reducibility of the catalysts.

The reducibility of the catalysts was investigated using H₂ (and CO)-TPR technique. Fig. 3 shows the H₂-TPR profiles obtained for the Ce-YSZ oxide and for the Cu/Ce-YSZ and Co/Ce-YSZ catalysts. In the case of Ce-YSZ support, water production (mass / charge ratio = 18) started at a temperature as low as 200 °C, in the form of a sharp profile peaking at 244 °C. The low-temperature reducibility of this oxide has previously been associated with its surface nature, which consists mainly of nanolayers

of $\text{Ce}_2\text{Zr}_2\text{O}_8$ with pyrochlore-like structure, and in particular with its ability to activate the hydrogen molecule, which is thought to be the rate controlling step in the overall reduction process [26, 27].

< near Figure 3 >

With respect to the reducibility of the Cu/Ce-YSZ and Co/Ce-YSZ catalysts, complicated TPR profiles with overlapping contributions were obtained. The onset of reduction occurs at 133 °C and 178 °C for Cu/Ce-YSZ and Co/Ce-YSZ, respectively. The TPR profile of the Cu/Ce-YSZ catalyst shows two sharp reduction peaks with maxima at 200 °C and 267 °C, followed by a broad band extending up to 700 °C. A small shoulder at the low temperature side of the first peak is also observed. The signal at 267 °C and the high temperature band could be assigned to the reduction of the Ce-YSZ oxide, according to the results obtained for the bare support. The low temperature shoulder and the signal centred at 200 °C would account for the reduction of CuO species.

On the other hand, the Co/Ce-YSZ catalyst shows a profile characterized by a maximum at 267 °C, presumably corresponding to the reduction of the support, and a second contribution formed by several overlapping reduction peaks centred at 400 °C, attributable to the transformation of Co_3O_4 into Co. The reducibility of Co_3O_4 has been extensively studied and many authors suggest that the spinel phase is usually reduced in a stepwise process, giving a low temperature peak in the range 200–300 °C, corresponding to the reduction of Co^{3+} to Co^{2+} , and a higher temperature one, at 400–500 °C, corresponding to the reduction of Co^{2+} to Co^0 [28,29].

The deconvolution of the TPR profiles in Gaussian type functions has allowed us to confirm the proposed reduction sequences. Thus, the interpretation of each peak can be made from the estimation of the ratio between its area and the total area, assuming that the samples become fully reduced after the TPR experiment. Thus, assuming that after TPR runs the samples are fully reduced (in form of Cu, Co and Ce^{3+}), the quotient between the area of the Gaussian peaks and the total area obtained for the $m/z=18$ signals can be used to assign the origin of each contribution. The results are shown in Fig. 3 and Table 3. In this table, the theoretical amounts of H_2O expected from the reduction of different

species (CuO, Co₃O₄, support) as well as the values obtained from the integration of the deconvoluted patterns are gathered.

The sum of the areas of the peaks 1,2 and 4 in the deconvoluted pattern of Cu / Ce-YSZ (solid gray line) represents an amount of water of 0.64 mmol H₂O/g_{cat}, very similar to that theoretically required for the complete reduction of CuO (0.66 mmol H₂O/g_{cat}). The reduction of CuO species at different temperatures may be associated with the presence of CuO crystallites of different sizes, in different locations and / or with different degrees of interaction with the support. [30,31]. Likewise, the amount of H₂O obtained from the integration of peaks 3 and 5 (dotted grey line, 0.50 mmol H₂O/g_{cat}) agrees with that calculated for the total reduction of Ce⁴⁺ to Ce³⁺ in the Ce-YSZ support (0.48 mmol H₂O/g_{cat}). The former could correspond to Ce⁴⁺ in Ce₂Zr₂O₈ nanoparticles, while the very large one centred at around 500 °C can be associated with a very limited amount of cerium cations in isolated CeO₂ particles.

Five contributions were also considered to decompose the H₂-TPR profile of the Co/Ce-YSZ catalyst. Peaks 2 and 5 would account for the total reduction of Ce⁴⁺ in the Ce-YSZ support (0.48 mmol H₂O/g_{cat}, dotted line). The remaining area (sum of peaks 1, 3 and 4) coincides quite closely with that expected for the reduction of Co₃O₄. The signal at 200 °C might account for the reduction of the smaller Co₃O₄ particles. On the other hand, the reduction peaks at around 300 °C and 400 °C would be associated with the consecutive steps to transform Co³⁺ into Co²⁺ and Co²⁺ into Co, respectively [28].

< near Table 3 >

The reducibility of the catalysts under CO atmosphere was investigated as well. The results corresponding to CO-TPR are shown in Fig. 4. In this case, the formation of CO₂ (m/z=44) was followed to monitor the reduction processes. As it can be seen on this Figure, the reducibility of Ce-YSZ by CO is not as high as that observed in the experiment with H₂. The CO-TPR profile obtained for this oxide shows a low intensity peak at 360 °C and a second one at about 730 °C, which can be

ascribed to different Ce^{4+} locations (with respect to the surface) in the $\text{Ce}_2\text{Zr}_2\text{O}_8$ layers, or to the presence of layers with different thickness.

< near Figure 4 >

With regard to Co/Ce-YSZ and Cu/Ce-YSZ catalysts, complex CO-TPR profiles were also observed that can be properly assigned to the constituents of the catalysts after deconvolution of the TPR signals (Fig. 4). Thus, in the case of Co/Ce-YSZ catalyst, the first three gaussian peaks resulting from this process can be ascribed to the reduction of the Co_3O_4 particles [32]. Once metallic Co is formed, it activates the reduction of the support, which occurs at 570°C (peak 4) in this catalyst. In the case of Cu/Ce-YSZ, the reduction onset occurs at lower temperature. Four consecutive peaks in the range $80\text{--}200^\circ\text{C}$ would account for the reduction of CuO, thus indicating the presence of different forms (locations, aggregates size, ...) of Cu^{2+} species in this sample [33]. The peak centred at 480°C can be ascribed in this case to the reduction of the support. These assignments demonstrate a good quantitative accordance between experimental (integrated area) and theoretical (calculated) values, for both support and metallic phase reduction processes involved, as shown in Table 4.

According to these whole results, it can be confirmed that the presence of metallic Cu or Co activates the reduction of the Ce-YSZ oxide by CO, as demonstrated by the displacement of its main reduction peak from 730°C (in the bare support) to 578°C and 278°C , for the Co/Ce-YSZ and Cu/Ce-YSZ catalysts, respectively.

<near Table 4>

3.3. Compositional analysis by EDS.

With the aim of exploring the distribution of elements in the catalysts investigated, energy-dispersive X-ray spectroscopy (EDS) analyses were carried out. EDS-mappings of Cu and Co catalysts are presented in Fig. 5 and 6, and the chemical composition obtained from the EDS spectra is shown in Table 5. In the case of Cu/Ce-YSZ (Fig. 5), the EDS mapping shows that Ce, Y and Zr are homogeneously distributed, while the Cu X-ray signal mainly comes from aggregates with different morphologies and sizes located at the surface of the Ce-YSZ particles. Fig. 6 illustrates a

representative image of the Co/CYSZ catalyst, as well as the EDS mappings for Co, Ce, Y and Zr. In this case, and probably due to the particle thickness, we can clearly identify the surface nature of Ce species, which appear mainly concentrated at the edges of the particle. Aggregates of Co, smaller in size than those observed for Cu, are also better dispersed on the particle surface and, therefore, in greater contact with Ce.

< near Figure 5 >

The overall chemical composition obtained from EDS (Table 5) does not coincide with the results obtained from ICP (Table 2), which is expected because the EDS analyses were taken in small areas surrounding Cu (or Co) metal particles, where the metal content is not representative for all the sample. However, the values obtained for the Ce/(Ce+Y+Zr) ratio are rather similar to those obtained by ICP, thus indicating a very good compositional homogeneity of the Ce-YSZ support also on a nanoscopic scale.

< near Table 5 >

3.4 Catalytic Activity measurements.

The NO to NO₂ oxidation activity of the selected catalysts was evaluated in Temperature Programmed Oxidation reactions (TPO) and Fig.7 compiles the NO₂ production profiles obtained as a function of temperature (solid lines). It is important to underline that the un catalyzed NO oxidation reaction occurred at very low extent under the same experimental conditions. The predicted NO₂ level considering the thermodynamic equilibrium of the NO oxidation reaction to NO₂ is also represented in the same Figure as a dotted black line, showing that this reaction is thermodynamically favoured at low temperatures but not at high temperatures.

< near Figure 7 >

The most remarkable feature illustrated on Fig. 7 is the outstanding activity of the cobalt-containing catalyst (solid orange line). Both the pattern and the maximum amount of NO₂ production achieved are similar to those shown by the commercial Pt-catalyst (but being a little bit lower) thus revealing

its high reactivity towards the mentioned oxidation reaction. The Co/Ce-YSZ synthesized presents a maximum NO₂ production activity higher than 70% and very close to that of Pt. The pronounced slope of the representation is very similar to that of Pt as well and differs considerably from the smooth slope observed for the copper-containing catalyst and the support.

It is worth commenting that one of the most active catalysts prepared until now was a sample consisting of nano-particles of ceria-praseodymia synthesized by a sophisticated surfactant-aided method based on the obtention of a reverse micro-emulsion [20]. The performance of the Co/Ce-YSZ catalyst is also remarkable in comparison with that shown by this Ce-Pr oxide (see corresponding comparative on Fig. S2 on Supplementary Information).

Fig. 8 depicts the soot conversions profiles versus temperature using the selected catalysts (solid lines) under the mode of *loose contact*. The implications of the NO₂ production capacity of the investigated catalysts on their soot combustion activities under NO_x+O₂ are very obvious for this series of catalysts. Since NO₂ is required to initiate and propagate the soot oxidation under *loose contact* conditions, the conversion of NO to NO₂ is an important step during catalytic soot combustion in the presence of NO and O₂ [34]. Even though some studies reported that for a set of Ce-Zr catalysts a direct relationship between NO₂ production and soot combustion was not found because of the contribution of the active oxygen-assisted mechanism, being more relevant as the reaction temperature is higher [35], for the present case reported (where some of the catalysts present remarkable activity for NO₂ production at low temperatures), the correlation is evidenced.

< near Figure 8 >

Nevertheless, the attempts to establish correlations among the redox activities (reducibility behaviour) of both transition metal-catalysts and the soot combustion performance failed. Some studies reported that direct relationships among easiness of catalysts' reduction under reducing atmospheres (monitored by TPR-H₂ or TPR-CO) and catalytic performance's under oxidative atmospheres are not fulfilled [36]. This is a clear example showing this lack of correlation. For the catalysts considered, a whole reduction is achieved both under H₂ and CO for the two supported

catalysts investigated in the TPR experiments. However, the reducibility is promoted to lower temperatures for Cu/Ce-YSZ with regard to Co/Ce-YSZ (under H₂ atmosphere) and more dramatically under CO atmosphere due to the different processes involved in both reactions. The own oxidised pyrochlore phase is characterized by a large ability to activate the H₂ molecule [26]. On the contrary, it can be accepted that the presence of metallic entities of copper and cobalt activates the reduction of the Ce-YSZ oxide by CO. In this sense, copper seems to be much more active in this system under CO presence than cobalt.

In an attempt to gain more insight into the reasons of the lack of correlation concerning reducibility properties and soot combustion activity, the corresponding soot combustion curves under a NO-free atmosphere (only containing 5% O₂) are displayed on Fig. 9. The observed activity trend is quite different to that found under NO_x/O₂ (in agreement with previous works comparing different sets of catalysts [37]) and now the Pt-based catalyst is the least effective, followed by Ce-YSZ, Co/Ce-YSZ and Cu/Ce-YSZ. Not surprisingly, these four curves move towards higher temperatures in the NO-free stream, due to the inoperativeness of the NO₂-assisted mechanism, again evidencing the role of NO₂ as originator and propagator of the soot combustion reaction under *loose contact*. If NO_x is absent, the order of soot combustion rate matches with the performance in reducibility. In other words, when the “active oxygen”-assisted mechanism is the only pathway governing the catalytic activity for soot combustion, the most reducible sample under H₂, but specially under CO, (that containing copper) is that most active under these experimental conditions, as seen by comparing Fig. 9 with Fig. 3 and 4. It is important to take into account that under CO-TPR the most important steps consist of the activation of the CO molecule and the corresponding transfer of O (from the own catalyst) to CO. An effective delivery and transfer of active oxygen from the catalyst to the soot surface are the main factors governing the soot combustion under O₂ alone as well [38,39].

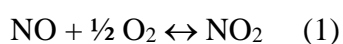
< near Figure 9 >

With the aim of exploring the specific mechanisms playing in the catalytic oxidation of soot and to investigate more deeply how NO₂ is specifically produced and effectively utilised in this reaction,

Fig. 10 A) represents the NO₂ slip percentage, which is the unreacted NO₂ emerging during a soot combustion experiment, in terms of temperature, for the three metal-supported catalysts (Pt, Co and Cu, in dotted lines). For comparison purposes, the NO₂ produced levels during the corresponding blank experiments (previously shown on Fig. 7, in solid lines) are also compiled.

< near Figure 10 >

It is worth of mention that even though the soot combustion is significantly accelerated in the case of the Pt-catalyst (Fig. 8), the difference between the NO₂ profile (obtained from a TPO experiment) and the NO₂ slip profile is very small (4% in the maximum, approximately). These ideas, joined to the lowest activity shown by the Pt-containing catalyst under O₂/N₂ stream, lead to assess that the high activity towards soot combustion originated by the noble metal catalyst is not only due to its highest NO₂ production. This remarkable activity is also attributed to the high effectiveness of the commercial Pt-catalyst to recycle the NO molecules derived from the NO₂-soot reaction again to NO₂, acting as source of NO₂ along the catalytic bed, thus providing these molecules continuously at a temperature relevant to be used for soot combustion, as reported in previous publications [33, 40-44]. Therefore, NO can have a catalytic role, as well, according to this global scheme of reactions proposed [34]:



Comparing now Co/Ce-YSZ and Cu/Ce-YSZ profiles on Fig. 10 A), an interesting indirect evidence can be deduced. Despite of the fact that the differences between the NO₂ produced in a blank experiment and the NO₂ slip in the soot-catalyst experiment are very similar for both catalysts (0.64 mmol NO₂/g_{cat} for the Co-containing catalyst and 0.60 mmol NO₂/g_{cat} for the Cu-containing catalyst), the soot combustion activity for the former is considerably more accentuated even though the potential active-oxygen assisted contribution to the whole activity is also lower (Fig. 9). A rational explanation for that is as follows: mainly for the case of Co/Ce-YSZ catalyst, the NO molecules are being used multiple times, in a similar way than Pt, but in a lower extension. This would explain the

significantly high combustion rate for this catalyst compared with its counterpart containing Cu and would imply a better utilization of NO_x for the soot combustion purpose. A better understanding of the catalytic function leads to conclude that the Co-containing catalyst is not only a better NO₂ generator than the Cu-containing catalyst but also exhibits a more efficient utilization of NO_x. Under a *loose contact* configuration of soot/catalyst, NO produced as a consequence of soot oxidation reaction (reaction 2) can go through the reaction cycles defined (1-2) and oxidise soot along the catalytic bed multiple times.

The impact of catalyst formulation and the role of the different components of the X/Ce-YSZ systems is evaluated now. For this purpose and trying to shed light on the reasons why the Co/Ce-YSZ catalyst is so active interacting with the NO molecules despite of their redox properties are worse than those showed by the Cu-catalyst, the corresponding metallic oxide phases found on both catalysts (Co₃O₄, spinel phase and CuO, tenorite phase, respectively) were synthesised by means of the corresponding nitrate precursors in order to obtain the bulk compounds and testing them in the catalytic reactions analysed.

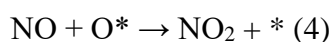
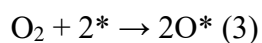
For comparative purposes with the supported-metal catalysts, the corresponding representations of the bulk phases were included as dotted curves on Fig. 8 and in a separate graph on Fig. 10B). Interestingly, the Co₃O₄ phase *per se* is an excellent NO₂ producer, better than its supported counterpart and this is reflected in an improved soot combustion activity as well, yielding a conversion profile curve very close to that of Pt. On the contrary, concerning CuO phase, even though its NO oxidation activity (blue dotted line on Fig. 10B) is better than that characteristic of the metal-supported version (Fig. 10A), its corresponding soot combustion profile is moved towards very high temperatures, and only from 550 °C on, (due to the presence of a higher amount of remaining soot in the catalytic bed), the soot combustion rate presents a pronounced slope.

Consistently with these sequences of soot combustion activity, the NO recycling efficiency of the Co₃O₄ phase is very high, suggesting a relevant function of the redox pair (Co²⁺/Co³⁺) to interact with NO multiple times along the catalytic bed. Conversely, the CuO phase has a null activity for this

function and NO₂ slip only emerges at very high temperatures (Fig.10B), coinciding with the nearly complete consumption of soot in the reactor.

The importance of the high efficiency of NO ↔ NO₂ ↔ soot cycle has been reported by some researchers [34, 39-43] but mainly in the context of Pt-based catalysts. It has been demonstrated that the NO₂ derived from NO oxidation would react with soot and initiate the creation of surface oxygenated complexes, (SOCs), which are more reactive than the complexes previously existing on soot's surface. As a consequence of this, both O₂ and NO₂ are able to react with SOCs to finally generate CO₂, which is also a crucial step for the catalytic oxidation of soot [42]. Therefore, if the recycling efficiency is high, this will provide more chances for the NO₂-soot reaction to generate these SOCs. The whole results obtained demonstrate that the Co₃O₄ entities are the main responsible (by themselves) of the high recycling function, and in turn, this leads to a high soot combustion activity under NO_x/O₂. In this context, Co₃O₄ unsupported or supported entities would act as a *pseudo-platinum phase* allowing fresh supply of NO₂ along the catalytic bed, thus accelerating the soot combustion reaction. As far as these authors are concerned, this finding is quite interesting, since, in general, non-noble metal catalytic phases (both unsupported or supported) are not so active in NO₂ recycling processes, and this can have a relevant impact on the soot combustion activity.

Previous works reported a fast NO oxidation turnover on large Co₃O₄ clusters [44,45]. In this sense, a high dispersion of Co₃O₄ entities was not a requisite in agreement with the present investigation. Co₃O₄ entities have been reported as a more active phase than CeO₂ or Ag for NO oxidation under O₂ presence [36]. Differently from CeO₂-based materials, which are expected to follow a Mars-van-Krevelen route for soot oxidation under O₂ presence, this possible route is completely overwhelmed when NO_x is present for the case of Co₃O₄ entities, yielding a higher NO₂-assisted soot combustion. NO was reported to be efficiently oxidized by these entities by following an Eley-Rideal mechanism [44]:



which was attributed to Pt-catalysed NO oxidation by some authors as well [46]. Hence, some of the different catalytic behaviors observed could be tentatively explained by mechanistic implications.

On the contrary, CuO bulk phase is not active in the NO₂ recycling reaction, even though its NO₂ production capacity is moderated. These experimental evidences are supported by the trend of the redox potential pairs. In fact, Co³⁺/Co²⁺ can be considered as a high electrochemical redox potential (1.92 V) [44], meanwhile Cu²⁺/Cu⁺ presents a potential of 0.13 V (not so highly oxidizing). Co₃O₄ could activate O₂ easily and thereby was a powerful NO oxidizer with a high recycling efficiency, similar to that exhibited by Pt.

4. CONCLUSIONS

In this work, copper and cobalt catalysts supported on a highly reducible cerium, yttrium and zirconium oxide have been prepared. The cobalt catalyst shows an excellent NO oxidation behavior, much better than that of copper and even comparable to that offered by a commercial platinum catalyst. It is equally more active than copper for soot oxidation in the presence of NO_x. According to the results obtained with the corresponding bare oxides (Co₃O₄ spinel phase and CuO tenorite phase), Co₃O₄ entities would act as a *pseudo-platinum phase* allowing fresh supply of NO₂ along the catalytic bed, thus accelerating the soot combustion reaction *via* a NO₂-assisted mechanism. When NO_x is absent, the order of soot combustion rate matches with the performance in reducibility, with the copper catalyst being the most active. In other words, when the “active oxygen”-assisted mechanism is the only pathway governing the catalytic activity for soot combustion, the most reducible sample is also the most active. Under these conditions, Ce-YSZ supported catalysts benefit from the excellent oxygen-exchange properties of surface Ce-Y-Zr oxide nanostructures.

ACKNOWLEDGMENTS

The authors thank the Ministry of Economy and Competitiveness of Spain (Projects MINECO/FEDER MAT2013-40823-R and CTQ2015-64801-R), the Junta Andalucía (FQM-110

group) and Generalitat Valenciana (PROMETEO/2018/076) for their financial support. Also, JCMM acknowledges Spanish Ministry of Education, Culture and Sports for the financial support through a FPU grant (FPU17/00603).

REFERENCES

- [1] T. Johnson, A. Joshi, “Review of Vehicle Engine Efficiency and Emissions” SAE Technical Paper 2018-01-0329, 2018.
- [2] M. Cortés-Reyes, C. Herrera, M.Á. Larrubia, L.J. Alemany, *Appl. Catal. B Environ.* 193 (2016) 110–120.
- [3] R. Kimura, J. Wakabayashi, S.P. Elangovan, M. Ogura, T. Okubo, *J. Am. Chem. Soc.* 130 (2008) 12844–12845.
- [4] Y. Yu, J. Ren, D. Liu, M. Meng, *ACS Catal.* 4 (2014) 934–941.
- [5] C. Cao, L. Xing, Y. Yang, Y. Tian, T. Ding, J. Zhang, T. Hu, L. Zheng, X. Li, *Appl. Catal. B Environ.* 218 (2017) 32–45.
- [6] J.M. Christensen, J.-D. Grunwaldt, A.D. Jensen, *Appl. Catal. B Environ.* 205 (2017) 182–188.
- [7] G. Yang, Y. Li, Y. Men, *Catal. Commun.* 69 (2015) 202–206.
- [8] M. Piumetti, S. Bensaid, N. Russo, D. Fino, *Appl. Catal. B Environ.* 165 (2015) 742–751.
- [9] T. Andana, M. Piumetti, S. Bensaid, L. Veyre, C. Thieuleux, N. Russo, D. Fino, E.A. Quadrelli, R. Pirone, *Appl. Catal. B Environ.* 209 (2017) 295–310.
- [10] N.D. Wasalathanthri, T.M. SantaMaria, D.A. Kriz, S.L. Dissanayake, C.-H. Kuo, S. Biswas, S.L. Suib, *Appl. Catal. B Environ.* 201 (2017) 543–551.
- [11] D. Fino, S. Bensaid, M. Piumetti, N. Russo, *Appl. Catal. A* 509 (2016) 75–96.
- [12] Y. Wei, J. Liu, Z. Zhao, Y. Chen, C. Xu, A. Duan, G. Jiang, H. He, *Angew. Chem. Int. Ed. Engl.* 50 (2011) 2326–2329.

- [13] F. Ji, Y. Men, J. Wang, Y. Sun, Z. Wang, B. Zhao, X. Tao, G. Xu, *Appl. Catal. B Environ.* 242 (2019) 227-237.
- [14] I. Atribak, A. Bueno-López, A. García-García, *Top. Catal.* 52 (2009) 2088–2091.
- [15] N. Guillén-Hurtado, A. Bueno-López, A. García-García, *J. Mater. Sci.* 47 (2012) 3204–3213.
- [16] Setiabudi, A., Chen, J., Mul, G., Makkee, M., Moulijn, J.A., *Appl. Catal. B Environ.* 51 (2004) 9-19.
- [17] Bueno-López, A., Krishna, K., Makkee, M., Moulijn, J.A., *Catal. Lett.* 99 (2005) 203-205.
- [18] I. Atribak, A. Bueno-López, A. García-García, *Top. Catal.* 52 (2009) 2088–2091.
- [19] E. Aneggi, C. De Leitenburg, J. Llorca, A. Trovarelli, *Catal. Today* 197 (2012) 119-126.
- [20] N. Guillén-Hurtado, A. García-García, A. Bueno-López, *Appl. Catal. B Environ.* 174-175 (2015) 60-66.
- [21] *In Catalysis by Ceria and Related Materials*, 2nd Ed. (Eds.: A. Trovarelli, P. Fornasiero), Imperial College Press, London, 2013.
- [22] T. Montini, M. Melchionna, M. Monai, P. Fornasiero, *Chem. Rev.* 116 (2016) 5987–6041.
- [23] L. Ai, Z. Wang, Y. Gao, C. Cui, B. Wang, W. Liu, L. Wang, *J. Mater. Sci.* 54 (2019) 4495-4510.
- [24] C. Arias-Duque, E. Bladt, M.A. Muñoz, J.C. Hernández-Garrido, M.A. Cauqui, J.M. Rodríguez-Izquierdo, G. Blanco, S. Bals, J.J. Calvino, J.A. Pérez-Omil, M.P. Yeste, *Chem. Mater.* 29 (2017) 9340-9350.
- [25] M. P. Yeste, J. C. Hernández-Garrido, D. C. Arias, G. Blanco, J. M. Rodríguez-Izquierdo, J. M. Pintado, S. Bernal, J. A. Pérez-Omil, J. J. Calvino, *J. Mater. Chem. A* 1 (2013) 4836-4844.
- [26] M. P. Yeste, J. C. Hernández-Garrido, S. Bernal, G. Blanco, J. J. Calvino, J. A. Pérez-Omil, J. M. Pintado, *Chem. Mater.* 18 (2006) 2750-2757.
- [27] M. P. Yeste, J. C. Hernández-Garrido, S. Trasobares, S. Bernal, G. Blanco, J. J. Calvino, J. A. Pérez-Omil, J. M. Pintado, *Chem. Mater.* 20 (2008) 5107-5113.
- [28] Z. Guchu, Xu. Yao, W. Shujie, C. Mingxia, S. Wenfeng, *Catal. Sci. Technol.* 5 (2015) 1084-1092.

- [29] C. Cao, L. Xing, Y. Yang, Y. Tian, T. Ding, J. Zhang, T. Hu, L. Zheng, X. Li, *Appl. Catal. B Environ.* 218 (2017) 32-45.
- [30] M. Zabilskiy, P. Djinović, B. Erjavec, G. Dražić, A. Pintar, *Appl. Catal. B Environ.* 163 (2015) 113-122.
- [31] Z. Luo, D. Mao, W. Shen, Y. Zheng, J. Yu, *RSC Adv* 7 (2017) 9732-9743.
- [32] J. Ajay, L. Yeol-Lim, J. Won-Jun, S. Jae-Oh, J. Kyung-Won, N. Hyun-Suk, K. Hak-Min, R. Hyun-Seog, J. Dae-Woon, J. Sang, N. Jeong-Geol, Y. Wang, *Mol. Catal* 433 (2017) 145-152.
- [33] Z. Wu, H. Zhu, Z. Qin, H. Wang, J. Ding, L. Huang, J. Wang, *Fuel* 104 (2013) 41-45.
- [34] A. Setiabudi, B.A.A.L van Setten, M. Makkee, J.A. Moulijn, *Appl. Catal. B Environ.* 351 (2002) 159-166.
- [35] I. Atribak, F.E. López-Suárez, A. Bueno-López, A. García-García, *Catal Today* 176 (2011) 404-408.
- [36] X. Wang, B. Jin, R. Feng, W. Liu, D. Weng, X. Wu, S. Liu, A robust core-shell silver soot oxidation catalyst driven by Co_3O_4 : Effect of tandem oxygen delivery and Co_3O_4 - CeO_2 synergy, *Appl. Catal. B Environ.* (2019), <https://doi.org/10.1016/j.apcatb.2019.03.019>
- [37] N. Guillén-Hurtado, F.E. López-Suárez, A. García-García, A. Bueno-López, *Reac. Kinet. Mech. Cat.* 111 (2014) 167-182.
- [38] N. Guillén-Hurtado, A. García-García, A. Bueno-López, *J. Catal.* 299 (2013) 181-187.
- [39] J. Giménez-Mañogil, A. García-García, *Fuel Process. Tech.* 129 (2015) 227-235.
- [40] A. Setiabudi, M. Makkee, J.A. Moulijn, *Appl. Catal. B Environ.* 42 (2003) 35-45.
- [41] S. Liu, X. Wu, D. Weng, M. Li, J. Fan, *Appl. Catal. B Environ.* 138-139 (2013) 199-211.
- [42] S. Liu, X. Wu, D. Weng, Y. Lin, M. Li, D. Weng, J. Fan, *Chin. J. Catal.* 35 (2014) 407-415.
- [43] S. Liu, X. Wu, D. Weng, M. Li, D. Weng, J. Fan, *Appl. Catal. B Environ.* 138-139 (2013) 199-211.
- [44] B. M. Weiss, N. Artioli, E. Iglesia, *Chem. Cat. Chem.* 4 (2012) 1397-1404.
- [45] Z. Ren, Y. Guo, Z. Zhang, C. Liu, P. Gao, *J. Mater. Chem. A* 1 (2013) 9897-9906.

[46] A. Russell, W.S. Epling, *Catal. Rev.* 53 (2011) 337-423.

Figure captions

Table 1. OSC values after reduction at 350 and 500 °C.

Table 2. Chemical Composition and Surface Areas.

Table 3. Results from H₂-TPR experiments.

Table 4. Results from CO-TPR experiments.

Table 5. Results from EDS-mappings.

Figure 1. Pore Size Distribution obtained by the BJH method.

Figure 2. XRD diffractograms of the catalysts investigated.

Figure 3. H₂-TPR diagrams for the catalysts investigated (peak deconvolutions are included in grey).

Figure 4. CO-TPR diagrams for the catalysts investigated (peak deconvolutions are included in grey).

Figure 5.- TEM images and EDS mappings of Cu/Ce-YSZ catalyst.

Figure 6.- TEM images and EDS mappings of Co/Ce-YSZ catalyst.

Figure 7. NO₂ production profiles during the blank experiments for the catalysts investigated.

Figure 8. Soot conversion curves obtained under *loose contact* mode (500 ppm NO_x/5% O₂/N₂) for the catalysts investigated and the bulk phases.

Figure 9. Soot conversion curves obtained under *loose contact* mode (5% O₂/N₂) for the catalysts investigated.

Figure 10. NO₂ slip profiles, obtained during soot combustion experiments under NO_x/O₂ for: A) the catalysts and B) the bulk phases (solid lines indicating NO₂ profiles obtained under blank experiments, without soot).